A field study of wind dominant single sided ventilation through a narrow slotted architectural louvre system

Paul D O'Sullivan[1], Maria Kolokotroni[2]

1.Cork Institute of Technology, Cork, Ireland. 2.Brunel University, Uxbridge, Middlesex, United Kingdom

Abstract An increasingly popular solution for ventilation that facilitates strategies such as night cooling is the provision of purpose provided ventilation openings comprised of horizontal slotted architectural louvres. Often these are employed in single sided ventilation strategies where there exists an irregular unsteady interaction of wind and buoyancy forces. This paper presents results from full scale experimental measurements of the macroscopic Air Change Rate (ACR) for an opening utilising an architectural slotted louvre in zero2020/NBERT, a National Building Energy Retrofit Testbed in Cork, Ireland. 2 slot louvre cases and 3 plain opening cases were investigated with 44 tracer gas concentration decay tests completed in a single cell isolated office space. The findings show that, for similar boundary conditions, the spectral characteristics of the velocity in the opening are modified by the introduction of the Slot Louvre. A non-dimensional analysis highlights stronger wind dominant aeration for the louvre than a plain opening having comparable overall facade opening dimensions. On average across the various cases measured, the slot louvre ACR were 6.5% higher compared with the plain opening ACR with even greater increases when considering comparable free opening area cases specifically. A sensitivity analysis using stepwise multiple linear regression also demonstrated a high correlation between ACR, wind speed and wind direction for the Slot Louvre. A comparison of existing single sided correlations showed lower prediction error for the plain opening cases than for the slot louvre. When considering the dimensionless exchange rate parameter, F_r, the published values for plain openings was comparable to those in this study but were too low in general for the slot louvre. An alternative value for this is suggested based on the field study measurements.

Keywords: zero2020/NBERT, slot louvre, field study, macroscopic ACR, dimensionless exchange rate, single sided

1 Introduction

Evidence also exists that current ambitious envelope and fabric oriented heating demand reduction strategies might result in an increased risk of extended periods of overheating in new buildings (Psomas et al. 2016). This is likely to also be an issue for ambitious building retrofits. In addressing this, consequently, the heat

removal potential of natural ventilation systems and their effect on internal environment is increasingly becoming a critical metric in selection of the final design and operation strategy, particularly for free running buildings (Chiesa and Grosso 2015; Aflaki, Mahyuddin, and Baharum 2016). Passive cooling by increasing natural ventilation rates has been shown to be an effective, energy efficient strategy to reduce unwanted cooling loads in buildings by up to 7.7% (Florides et al. 2002). Extended monitoring has shown that naturally ventilated buildings typically use less than 50% of the corresponding energy consumption of air conditioned buildings and assessment of ventilative cooling techniques in Europe have shown they may contribute highly to reducing the cooling needs of buildings and be an effective tool for tackling climate change adaptation in existing buildings (Maria Kolokotroni, Kukaida, and Perera 1996; Maria Kolokotroni and Warren 2008). In recent years, the verified performance of various natural ventilation components used in passive cooling systems and strategies has recieved increased attention in the research literature (Belleri, Lollini, and Dutton 2014; Moosavi et al. 2014; Q. Chen 2009).

Table 1: Nomenclature

Nomenclature		**Greek Symbols**	
a	regression intercept	α	jet spread coefficient
A	Area	β	frequency power exponent
Ar	Archimedes Number	ω	frequency
b	regression predictor variable	θ	wind incidence angle
C_d	Orifice Discharge Coefficient	ϵ	residual error
C_P	Wind pressure coefficient	σ	variance, root mean square
CF	Dascalaki Correction factor	Δ	delta, difference
d	Fourier transform	ρ	density
F	Dimensionless Flow number	ϕ	wind azimuth angle
g	gravitational acceleration	**Subscripts**	
Gr	Grashof Number	e	external, eddy
h	height of opening	i	internal
I	1D Turbulence Intensity	m	measured
j	number of cycles per unit time	l	local, boundary
l	opening width	o	opening
n	total number of samples	r	reference, roof
p	total pressure	w	wind
P	reference pressure	**Acronyms**	
Q	volumetric flow rate	ACR	Air change rate(s)
Re	Reynolds Number	ACH	Air change per hour
r	2D unit vector	W,L,P	Windward, Leeward, Parallel
R^2	goodness of fit	L(1,2)	Louvre case
$\hat{R}^2$	adjusted R^2	P(1,2,3)	Plain opening case
$S(\omega)$	Power Spectrum	rmse	root mean squared error
T	Temperature	mse	mean squared error
t	time interval	mape	mean absolute percent error
U	velocity, wind speed	OLS	Ordinary Least Squares
x	parameter, discrete sample		

For deep retrofit projects enhanced single sided ventilation can be a viable option as it does not require substantial internal reconfiguration and is physically non invasive. In such strategies both inlet and exhaust must be positioned at the same facade with openings often positioned at high and low levels maximising buoyancy driven aeration. Achieving this maximum available height may not be possible in refurbishment situations where ventilation pathways are physically constrained by the existing fenestration apertures (Ma et al. 2012). Further to this, the physical size of ventilation openings is often limited by practical issues such as draughts and manual opening mechanisms. An increasingly popular solution to overcome these issues, that also facilitates strategies with demonstrated high potential for ventilative cooling in climates similar to Ireland, such as night cooling (Artmann, Manz, and Heiselberg 2007; M Kolokotroni and Aronis 1999), is the provision of purpose provided ventilation openings comprised of vertical or horizontal external architectural louvres, providing protection against burglary and rain ingress while providing sufficient opening area for aeration. However, while louvred vents are common in many engineering applications there exists little experimental data demonstrating their performance when subject to the interactions present in single sided ventilation of internal spaces.

1.1 Envelope flow through slotted openings

In cases with only a single unobstructed opening in an otherwise near sealed room, studies have shown that when the wind is present there exists a shear mixing layer, promoting turbulent eddy penetration. The existence of this acts as the primary airflow exhange mechanism at the opening, rather than the mean pressure difference normal to the opening driving flow (Yamanaka et al. 2006). Wind gustiness can also lead to the presence of a pulsating flow (Cockroft and Robertson 1976). Due to the importance of opening geometry, the introduction of a slotted louvre component (figure 1 & 2) would suggest a modification in how buoyancy and momentum forces will interact at the aerating opening. Published experimental work measuring macroscopic ACR across louvre/slot like systems appears limited. Argiriou et al (2002) investigated the impact of external tilted venetian blinds on the airflow across large openings using full scale testing and proposed a correction coefficient based on Archimedes number, Ar (Dascalaki et al. 1996). Koffi et al (2015) considered the effect on aeration performance using an acoustic shutter, effectively creating staggered pathways through a double skin opening. They found the shutter reduced ventilation rates by 72% but did not consider how the forces generating flow were modified. Recently Lee et al (2015) measured the pressure loss rate through exterior venetian blinds and found the blinds can alter the velocity by about 50%. However, these measurements were based on cross ventilation, had a separation space between the blind and opening and did not consider low wind incidence angles. Hughes et al discuss the importance of louvre design in commercial wind towers with

louvre angle and length important factors in directing airflow into the internal space while reducing resistance to flow (Hughes, Calautit, and Ghani 2012) though they did not investigate a system where the flow is often parallel to the louvered opening and within the building envelope rather than at roof level. In a different application concerned with obstruction spacing patterns affecting airflow Mara (2014) considered whether a solidity ratio alone, similar to the principle of net free area ratio in envelope openings, was sufficient for estimating drag coefficients for lattice type structures, finding that the spacing pattern was also an important parameter requiring consideration. There appears to be a lack of full scale experimental data for ventilation rates through integrated louvre systems. Other studies concerning flow interactions along perforated plates, arguably an idealised representation of the slot louvre, considered either a flow normal to the main perforated face or, where it does consider flow parallel to slotted or perforated cavities, the slotted openings were either; oriented normal to the direction of shear flow rather than with or parallel like a typical architectural louvre in a building envelope (similar to that considered here) (Sever and Rockwell 2005), or were sive like (Ekmekci and Rockwell 2003).

The objective of this paper is to present results from a field study of macroscopic ACR for an opening utlising an architectural slotted louvre in a low energy retrofit building scenario. A non-dimensional analysis is employed to categorize tests according to driving forces; a spectral analysis of velocities at the opening is then used to investigate any changes in the wind characteristic in the opening and energy distribution with the addition of a slot louvre. A number of existing semi-empirical correlations are compared with measurement results and, following a discussion about potential causes for the pattern of measured ventilation rates, a new dimensionless exchange rate parameter is suggested for improved modelling of wind dominant macroscopic flow through the louvre components.

2 Materials and Method

2.1 Field Study: slotted louvre opening

In 2012 Cork Institute of Technology in Ireland (CIT) completed the construction phase of zero2020/NBERT, a pilot project/research testbed for the low energy retrofit of their existing $29,000m^2$ teaching building originally constructed in 1974 (http://www.zero2020energy.com). The ventilation solution for the retrofit consists of a flush faced external louvre system, (Figure 1). Each slot louvre section comprises 17 air inlet slots with a facade porosity of 0.057% and a net free opening area, A_o, for each section of $0.107m^2$. Ventilation is supplied using dedicated insulated doors inside the slot louvre which are controlled either manually or

automated based on environmental conditions in the enclosed spaces. The anodized aluminium slot louvre has a 47% net free open area for airflow and each vertical louvre bank, comprised of two sections, has overall structural opening dimensions of 0.30m (w) x 1.60m (h). Each louvre slot also incorporates a unique concave shape which acts as a guiding component to incoming air, (see Figure 1 and 13). Under normal operation there are two louvre banks in the test space. A recent study investigated the system under "normal operation" mode with internal insulated doors remaining in place and in the open position, the full 2 louvre bank arrangement for the test space retained and a range of high/low opening configurations (P. D. O'Sullivan and Kolokotroni 2014). The study compared the system to an existing opening window in the pre retrofit space and the results showed comparable performance with improved internal envrionment. The objective of the study presented in this paper is to measure mean ventilation rates for a single, isolated, slot louvre section directly and compare this to a plain open aperture with comparable geometric dimensioning under various full scale boundary conditions. To aim is to infer any modifications to local airflow exchange mechanisms at the opening and investigate the ability of existing semi empirical correlations in adequately predicting the ACR measured. To achieve this an existing west facing, first floor, isolated single cell office space in zero2020/NBERT was utilised for experimental testing and data collection (Figure 4 and 5). A single structural opening was used for all test cases with overall dimensions, 0.76m x 0.30m, Figure 2. Two opening types were tested, a slot louvre, denoted L, and a plain aperture, denoted P, with 5 cases in total, 2 for the slot louvre openings and 3 for the plain opening, each with varying overall dimensions. Table 2 presents information relating to each opening case for the purposes of comparison of opening geometry.

Table 2: Geometric dimensioning information for each of the opening cases measured in the field study. Aspect Ratio, AR, based on individual louvre slots for L cases with 17 slots in total within the louvre for airflow passage making up the available **free** opening area. subscript 's' denotes slot.

Case	$\mathbf{H}_o$	$\mathbf{H}_s$	W_o	**AR**	$\mathbf{A}_o$
$(-)$	(m)	(m)	(m)	(H/W)	(m^2)
L1	0.76	0.021	0.30	0.07	0.107
L2	0.76	0.021	0.15	0.14	0.051
P1	0.76	-	0.30	2.53	0.228
P2	0.76	-	0.15	5.06	0.114
P3	0.38	-	0.30	1.27	0.114

A blanking plate was inserted to facilitate the reduced opening dimensions for some of the cases (Figure 2). In total 44 independant ACR tests were completed from 27th August 2014 to the 20th September 2014 with varying amounts of tests completed each day (3 on average) and no testing on some days. During each test various internal, local external and meteorological parameters were measured.

Figure 1: Left: Louvre module used for testing. Middle: louvre opening. Right: External facade of the testbed building showing the pre and post retrofit (see http:/www.zero2020energy.com for more details). Integrated vertical slotted louvre banks also visible

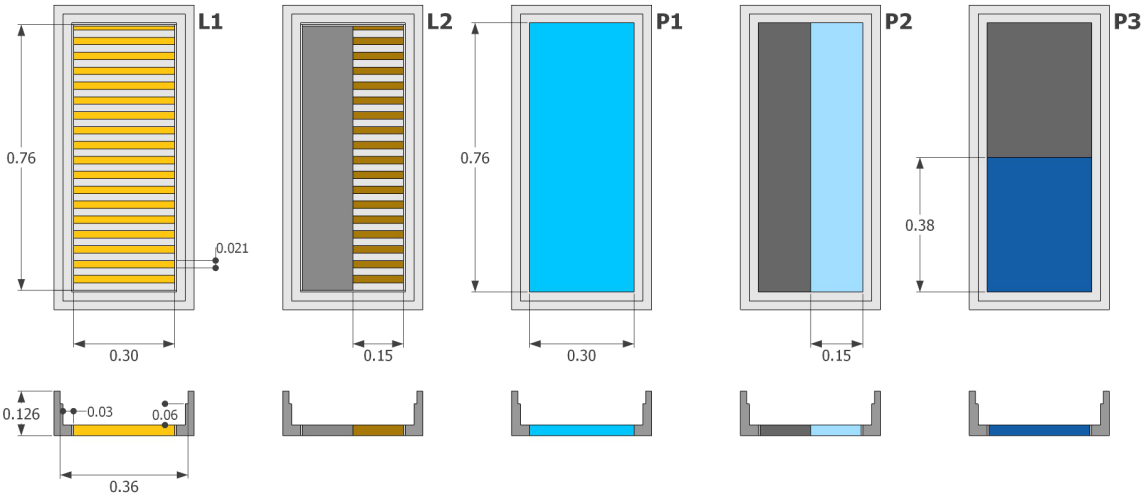

Figure 2: Plan and elevation drawings of various opening types measured including main dimensioning. Net free opening area for each case, A_o, shown coloured. Slot louvre, L, with 2 cases, L1 & L2. Plain opening, P, with 3 cases, P1, P2 & P3. Blanking plates used to create reduced H_o, W_o dimensions shown in dark grey

2.2 Experimental setup

Figure 4 provides information relating to instrument setup and positioning in the experimental test space and Figure 5 shows some of the installed instrumentation during testing.

2.2.1 ACR measurement

Macroscopic ACR during test periods were measured using the tracer gas concentration decay technique (Roulet 2007). Carbon Dioxide, CO_2, was chosen as the tracer gas for this work due to the ease of use, availability of analysis equipment, its density being similar to that of air and cost. Cui et al (2015) recently showed that using the concentration decay method with 6 in situ sensors provides ACR measurements with an uncertainty of between 6.8 and 15.6% when compared to a reference measurement using duct mounted airflow measuring blades (cases 3,4 and 5 in Cui et al). In the study presented here tests were completed in accordance with the procedures set out in ASTM E741-11 (ASTM 2011). All CO_2 concentrations were measured using AlphaSense IRC-A1 Non Dispersive Infra-Red (NDIR) Sensors. One external ambient, One adjacent corridor (the door was closed during testing) and Four internal zone CO_2 concentration measurement locations were used with a spatially averaged zone concentration calculated for estimating mean macroscopic ACR. A maximum 10% deviation between a particular location and the average zone concentration in accordance with section 12.4.1 of ASTM E741-11 was used to determine when there had been sufficient gas mixing (aided with a portable fan) prior to commencement of each test. CO_2 was injected from a single location using a liquid CO_2 cylinder and heat regulator. ACR were subsequently calculated using the linear regression decay technique (Sherman 1990), Eq. (1), with the normalised concentration, Eq. (2), from (ASTM 2011). Table 3 includes the mean, standard deviations and maximum values for the percentage difference between the measured concentration from a particular CO_2 sensor and the spatially averaged concentration for the zone at the beginning of each test, based on data from all 44 tests completed. Results shows good levels of mixing for all tests minimising measurement uncertainty due to imperfect mixing. Figure 3 presents decay profiles for a typical ACR test. To further reduce measurement errors influencing ACR the optimum concentration decay period for each test, t_m, was obtained based on the lumped parameter term, Nt_m, suggested by Okuyama & Onishi (2012). Here N is taken as the measured ACR value calculated from the concentration decay. For the number of measurement points, n, greater than 60, Nt_m tends monotonically to 1.25. We iteratively solved for Nt_m in each test and subsequently selected the corresponding time period satisfying this criteria, taken to be the optimum decay period and used for the calculation of ACR. The resulting mean n was 165 points with only 3 tests having values below 60. Again Figure 4 shows all instrument positioning referenced in Table 3.

$$lnC_N = -(ACR)t + lnC_N(0) \tag{1}$$

$$C_n = ln\frac{C(t) - C_0}{C(0) - C_0} \tag{2}$$

Table 3: Summary statistics for CO_2 uniformity of concentration across all 44 tests in accordance with ASTM E741-11. (% difference between individual location and spatially averaged concentration). Also shown for windward and leeward tests separately. See figure 4 for sensor positioning.

Parameter	**NW**	**NE**	**SW**	**SE**
Mean (All)	1.0%	1.7%	1.6%	1.1%
σ (All)	2.6%	2.3%	1.6%	2.4%
Max (All)	5.4%	8.6%	6.9%	5.7%
Mean (Windward)	0.3%	1.0%	1.2%	0.5%
σ (Windward)	2.3%	1.8%	1.9%	1.8%
Mean (Leeward)	1.5%	1.9%	1.7%	1.6%
σ (Leeward)	2.6%	2.3%	1.6%	2.5%

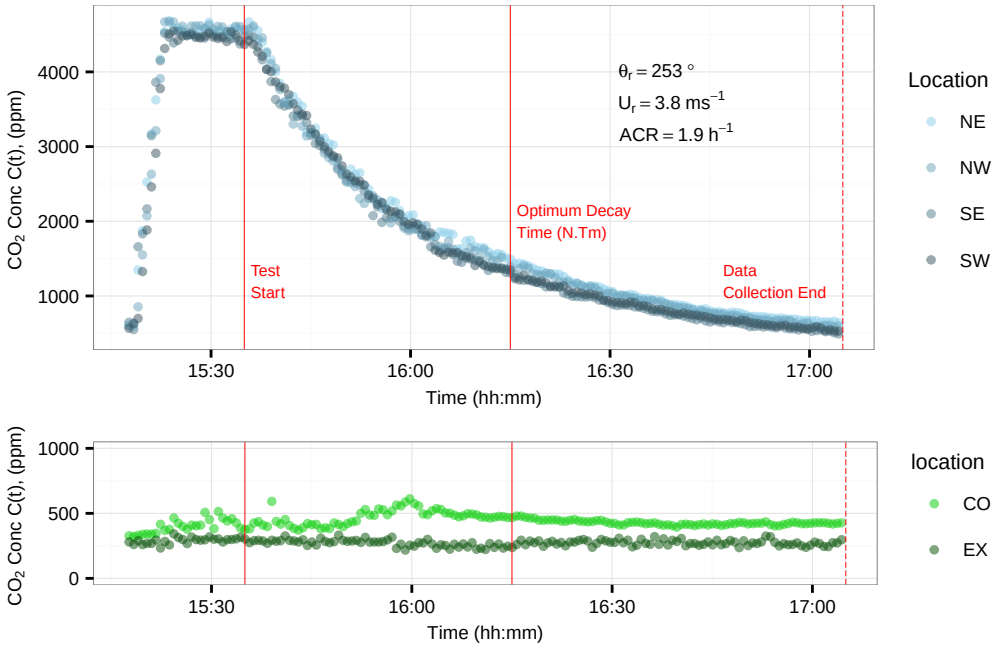

Figure 3: Typical CO_2 decay profiles (Test 35, 11th Sept 2014, case P2). Test start time, Optimum decay Time and data collection end time shown as vertical red lines. CO is adjacent corridor CO_2 sensor and EX is external CO_2 sensor. Figure 4 shows sensor locations

2.2.2 Internal and ambient parameters

Air speed in the opening was measured in 4 locations using E+E Elektronik EE576 miniature thin film anemometers ($\pm 0.08 ms^{-1} + 4\%$ measuring velocity) at a sampling rate of $1Hz$. Measuring locations varied horizontally to accommodate different opening heights and widths according to the test case but remained consistent for each case test subset and wind direction. Air temperature was measured in 8 locations within the zone using Hanwell Radio-logger RL4000 wireless data loggers with precision thermistors (± 0.1°C between -25°C to 50°C) at a sampling rate of 1 minute. Air temperature at the opening was also measured at 4 locations similar to the air velocity measurement locations using the same precision thermistors. Ambient temperature was measured at the roof using a Rotronic HC2-S3 probe. Wind data was collected during each test at three locations. Firstly, wind data was obtained from the local met station at Cork Airport for each test period, for comparative purposes. Secondly, at a height of 6.0m above the roof of the test room a Campbell Scientific 05103 wind vane anemometer sampling every 5 minutes (this was used to calculate the mean reference wind speed, U_r, for each test). Table 4 below provides summary statistics for wind and temperature conditions categorised according to opening case.

Table 4: Summary of external weather conditions during testing categorised according to each opening case. Conditions during testing for each case were comparatively equal for all boundary conditions.

Case	**Tests**	$\bar{U}_r$	σ_{U_r}	$\bar{\phi}_r$	$\bar{T}_e$	σ_{T_e}	$\Delta\bar{T}_{i-e}$
$(-)$	$(-)$	(ms^{-1})	(ms^{-1})	$(^\circ)$	$(^\circ C)$	$(^\circ C)$	$(^\circ C)$
L1	11	3.7	1.9	178	17.2	0.9	5.6
L2	9	3.1	1.7	179	17.3	1.5	5.9
P1	8	3.3	2.1	194	16.9	2.0	5.9
P2	7	2.7	0.8	137	18.0	1.8	5.4
P3	9	2.8	1.1	130	18.0	1.5	5.8

Finally, at 1.0m from the building envelope directly outside the ventilation opening a RM Young 81000 3D ultrasonic anemometer operated in uvw mode to allow for calculation of turbulence characteristics and local velocity data at sufficiently near to the opening to represent boundary conditions, with a sampling rate of $10Hz$. Eq. (3) is used to calculate the mean resultant vector, $\bar{r}$, in the 2D dimensional plane from the measured u, v components:

$$\bar{r} = \frac{1}{n}\sum_{i=0}^{n} r_i \tag{3}$$

where the individual unit vectors, r_i can be defined as Eq. (4) with $\cos\phi_i$ taken as measured u and $\sin\phi_i$

taken as measured v. The mean local orthogonal wind direction $\bar{\phi}$, is then calculated using the arctangent, from Eq. (5), and converted from radians to degrees. To correct for the $atan2$ function used for the arctangent we transform for $\bar{\phi} = \bar{\phi} + 360°$ if $\bar{\phi} < 0$ and $\bar{\phi}$ otherwise. This data, together with U_r is used to investigate the ratio U_l/U_r, a ratio used by various researchers in single sided correlations.

$$r_i = \begin{pmatrix} \cos\phi_i \\ \sin\phi_i \end{pmatrix} \tag{4}$$

$$\bar{\phi} = \frac{\pi}{2} \; - \; tan^{-1} \; (\bar{r}) \times \; \frac{180}{\pi} \tag{5}$$

3 Existing correlations

One of the main motivations for natural ventilation research is the development of accurate prediction techniques to account for the additional installation effects from turbulent wind. A number of different approaches and models exist to account for this local flow condition, when wind and buoyancy are simultaneously present. Bernoulli orifice theory is generally adopted as an acceptable theoretical basis when concerned with correlations for predicting macroscopic ACR through small, sharp edged openings.

3.1 Existing theory

Buoyancy alone envelope flow models rely on the principle of the still air discharge coefficient, C_d, with the assumption of independence from Reynolds number, Re, when dealing with envelope flows. Mean pressure differences generated across the opening from wind and buoyancy will result in a mean volumetric flow. These pressure differences across the envelope opening can be summarised using Eq. (6):

$$\Delta p = P_e - P_i - \Delta\rho g h + p_w \tag{6}$$

Introducing C_d and the area of the opening(s) we obtain a general theoretical model for steady envelope volumetric flow rate, Eq. (7):

$$\bar{Q} = C_d A_o \cdot \sqrt{| \; \frac{\Delta\rho g h}{2} + \frac{\Delta p_w}{2} \; |} \tag{7}$$

Using different forms of equation (5) depending on the case of interest different researchers have attempted to include additional experimentally derived factors to account for the complicated installation effects from turbulent wind, gustiness, opening geometries and wind incidence angle. It follows a summary of such existing correlations:–

- Warren: Warren and Perkins (P. R. Warren and Parkins 1985) were amongst the first researchers to investigate the jet mixing layer theory for building envelope flow. Their work sought to establish theoretical estimates of a dimensionless flow that incorporated how the shear mixing layer spreads along the opening. They proposed the relationship Eq. (8) with α suggested as having values of somewhere between $1.60 - 1.71$ for a highly turbulent three dimensional mixing layer. Based on field studies and subsequent wind tunnel tests they established a more suitable value for F_l of 0.1.

$$F_l = 0.056 \cdot \alpha \tag{8}$$

- Adams: Adams et al (2014) updated Warrens approach by adjusting the spread rate of a non symmetric turbulent jet that generates a shear mixing layer spreading along the horizontal length of the opening normal to the envelope. Based on work published by Dimotakis (2005) showing 70% of the outside air is entrained and Yamanaka (2006) suggesting new values for the relationship between U_l and Q_w Adams et al suggested an alternative α value to deal with the jet spread rate resulting in a value of $F_l = 0.075$.
- Argiriou: Dascalaki (1996) and more recently Argiriou (2002) used the Archimedes number and an experimentally dervied correction coefficient in lieu of C_d entirely for their empirical correlation.
- Larsen: Some models such as Pfaff & DeGids (1982) and Larsen & Heiselberg (2008) incorporated mean wind pressure, buoyancy and a turbulent component to their correlation using regression coefficients from wind tunnel and full scale measurements.
- Caciolo: Caciolo et al (2013) and more recently Tang et al (2016) proposed improvements for leeward conditions, predicting effective envelope temperature differences that allow for localised interactions with the wind depending on speed, incidence angle and magnitude of temperature difference respectively.

Alternatively to the approaches above Wang and Chen (2012) proposed a method that decomposes the mean and fluctuating velocity components and calculates separate contributions to the fluctuating component based on both pulsation flow and eddy penetration. For the present study Table 5 summarises correlations included for the purposes of comparison with experimental data. Further to the correlations outlined above an important requirement for many existing wind driven models is to use the reference wind velocity, U_r,

directly for calculation of ACR or alternatively predict the local velocity at the opening given some knowledge regarding U_r. Warren experimentally investigated this. They used a wind tunnel experiment to establish the relationship U_l/U_r as a function of wind incidence angle, θ, shown in figure 6 as discrete black points. Using these values they then transformed measured values of U_r taken during full scale ACR tests. They suggested based on the U_l/U_r results that this ratio will unlikely go below 0.25 and designers can adjust accordingly for Q_w in Table 2 by using an F_r value of 0.025 for smooth flow and 0.035 for a turbulent flow field. Chu recently found that F_r could be as low as 0.0175 (Chu, Chen, and Chen 2011).

Table 5: Existing Semi Empirical Models for Single Sided Ventilation used for comparison with field study ACR data recorded at zero2020/NBERT

Corr	Year	Formulae	Notes
Warren	1985	$Q_w = 0.1A_o\left(\frac{U_l}{U_r}\right)_\theta U_r$; $Q_{th} = \frac{1}{3}C_d A_o\sqrt{\frac{\Delta T_{ie} hg}{\bar{T}}}$	$Q = \max\left[Q_w, Q_{th}\right]$
Argiriou	2002	$Q = C_c A_o Q_{th}$; $C_c = aAr^b$ $a = 0.16 \pm 0.09$, $b = -0.25 \pm 0.07$	(Dascalaki et al. 1996)
Larsen	2008	$Q = A_o\sqrt{C_1 f(\beta)\sqrt{\mid C_p \mid}U_r^2 + C_2\Delta Th + C_3\left(\frac{\Delta C_{p,ope}\Delta T}{U_r^2}\right)}$	(Gids and Pfaff 1982) $U_l = f(\mid C_p \mid)$
Caciolo	2011	$Q_{th} = \frac{1}{3}A_o C_d\sqrt{\frac{\Delta T_{ie}\Delta T^* hg}{\bar{T}}}$; $Q_w = 0.0357A(U_w - U_{w,lim})$; $\Delta T^* = 1.355 - 0.179U_w$; $\Delta T^* = 1.234 - 0.490U_w + 0.048U_w^2$	$Q = Q_{th} + Q_w$; $U_{w,lim} = 1.23ms^{-1}$

Adams et al compared the velocity ratio of Warren to their own wind tunnel studies. Their results agreed well with Warren. They considered 9 different cases in total and from this they proposed Eq. (9) to predict U_l from θ given U_r.

$$U_l/U_r = 0.527 \cdot exp(-0.000638(\theta - 62)^2) + 0.25 - 0.00028\theta \tag{9}$$

As an alternative approach Larsen and Heiselberg suggested using an empirically derived 4th order polynomial describing the relationship between the wind pressure coefficient data for the opening of interest and the velocity ratio $(U_l/U_r)/\sqrt{\mid C_p \mid}$. This fitted model can then be used to predict U_l once the C_p data and U_r are both available. Using the C_p value to estimate the velocity ratio is useful as there are a number of existing sources for these values, often based on simplified geometries. Recently it was shown that there is up to only 15% difference on predicted ventilative cooling performance for natural ventilation models using C_p depending on the source (Ramponi, Angelotti, and Blocken 2014). Their results show favourable predictions

for the opening studied in the wind tunnel. The fitted model was based on Warren and Parkins data.

$$U_l = f(\beta) \cdot \sqrt{\mid C_p \mid} \cdot U_r \tag{10}$$

4 Experimental Data & Results

4.1 Local / reference velocity ratio

Figure 6 shows polar plots for $\bar{U}_r$ and incidence angle $\bar{\theta}_r$ (converted from $\bar{\phi}_r$), during each test at three locations; the local met station Cork Airport, the building roof level, and at the test opening, U_l. It is apparent that for almost all wind incidence angles the local direction of flow was almost always parallel. Figure 6 also compares measured U_l/U_r ratios as a function of $\bar{\theta}_r$ for each test plotted using a polar axis. U_l/U_r values recorded by Warren in a wind tunnel study are included in green for comparison (P. R. Warren and Parkins 1985) as is the results from Adams equation 9. Similar magnitudes to Warren at 315°is observed while greater magnitudes were consistently found at 0°compared with Warren and Adams; the results between 180°and 270°present no clear trend other than the fact they are all at or below the values measured by Warren and closer to those proposed by Adams. Some good agreement was also seen at 90°. Large U_l/U_r values were well correlated with large reference wind speeds (shown by the size of the data point) for windward incidence angles but for leeward incidence angles even with large U_r values low U_l/U_r ratios are regularly observed. The measurements suggest that simplified wind tunnel studies cannot easily predict the local velocity when there are additional effects from surrounding obstacles and terrain and confirm the strong dependancy on wind incidence angle.

4.2 ACR

Figure 7 presents measured macroscopic ACR, Q_m, associated with each test case. Values are binned at $0.25h^{-1}$. Wider distributions with higher mean values for L1 & P1, with low σ values for L2, P2 & P3 can be observed. The L type openings have a combined mean ACR of $2.13h^{-1}$ whereas the P type openings have a mean value of $2.0h^{-1}$ an average increase of 6.5% for L type openings. However, a more direct comparison, considering openings with the same overall facade opening dimensions, L1 has mean ACR of $2.5h^{-1}$, with P1 having $3.4h^{-1}$ giving an average reduction of 29%. L2 has mean ACR of $1.67h^{-1}$ with P2 having a value of $1.44h^{-1}$. However, the 3rd Quartile value for P2 is $1.5h^{-1}$ while for L2 it is $1.3h^{-1}$. P3 had a mean value of $1.24h^{-1}$. For the same opening height and reduced opening width, W_o, giving the same available free

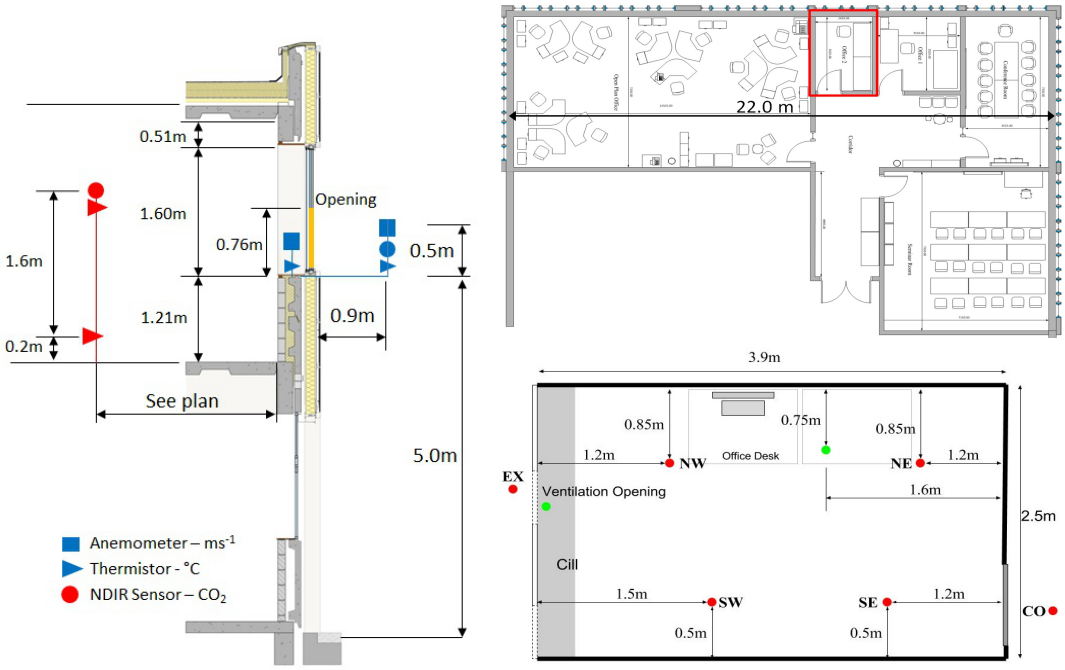

Figure 4: Experiment setup details. Left: Building section showing heights and depths of instrument positions. Right top: Overall testbed first floor plan with test room marked in red. Right bottom: Dimensions of CO_2 and Temperature measuring locations

opening area, A_o, (effectively comparing L1 with P2) a 78% improvement in ACR with the slot louvre is measured. Retaining the same opening length but reducing the available height to provide the equivalent net free area (effectively comparing L1 with P3), results in an 100% improvement using the slot louvre. In general for the study objectives only 1 section of the 4 section in the 2 louvre bank arrangment in the room. ACR would have been higher for normal operation. It is not possible to correct for differences in boundary test conditions for each measured ACR value as presented in figure 6 leaving a certain ambiguity as to the causality behind the distributions. Therefore, a Warren plot is used to separate individual test results that are buoyancy dominant from those that are wind dominant. Figure 7 presents a Warren Plot of all tests for the two different opening types. Warren plots have previously been used by researchers to analyse ACR data in this way, for example see (P. R. Warren and Parkins 1985; Caciolo, Stabat, and Marchio 2011; Van der Mass 1992; Paul D O'Sullivan and Kolokotroni 2016).

The Archimedes Number, Ar, is used as a measure of the relative magnitudes of the buoyancy forces and the momentum/inertial forces acting on the elements of fluid. The dimensionless exchange rate parameter, F_r, is a practical dimensionless number based on a reference wind velocity to characterise the quantity of wind induced ventilation for a given situation. Where flow is buoyancy dominated F_r should approach the

Figure 5: Instrument set up. Left: 3D Ultrasonic anemometer measuring boundary conditions. Middle: Typical opening case with E+E thin film anemometers measuring velocity. Right: internal layout and test room set up

asymptote defined by F_{th} in Figure 8. The sensitivity of conclusions drawn from a Warren Plot to the location of this F_{th} asymptote have been presented in (Paul D O'Sullivan and Kolokotroni 2016) showing, for orifice flow theory, high sensitivity at F_r values of around 0.03-0.04 and Ar around 0.12 upwards. For low Ar this is less of a concern. When wind dominates $Ar^{0.5}$ tends to zero and F_r becomes independent of $Ar^{0.5}$. For parallel flows, according to work by Warren (1985), F_r should be approximately constant at 0.03 though as mentioned before Chu suggested this value could be as low as 0.0175 (2011). F_r and Ar can be defined in Wq. (11) and Eq. (12) as:

$$Ar = \frac{\Delta T_{ie} hg}{\bar{T} U_r^2} \tag{11}$$

$$F_r = \frac{Q_m}{A_o U_r} \tag{12}$$

We can note the following observations from Figure 8:–

- The plot suggests a higher F_r range for the L opening cases for a given U_r and $Ar^{0.5}$, somewhere between 0.03 - 0.15 depending on opening dimensions and θ_r versus 0.025 - 0.1 for P opening cases.
- The slot louvre displays increased independence from $Ar^{0.5}$ suggesting the louvre cases at the opening height tested rely more on momentum than buoyancy forces.
- Increasing reference wind speed generally results in lower $Ar^{0.5}$ values and higher F_r irrespective of opening case.
- Similar distributions of $Ar^{0.5}$ values are present in all opening cases suggesting similar boundary conditions across all test cases with varying performance.

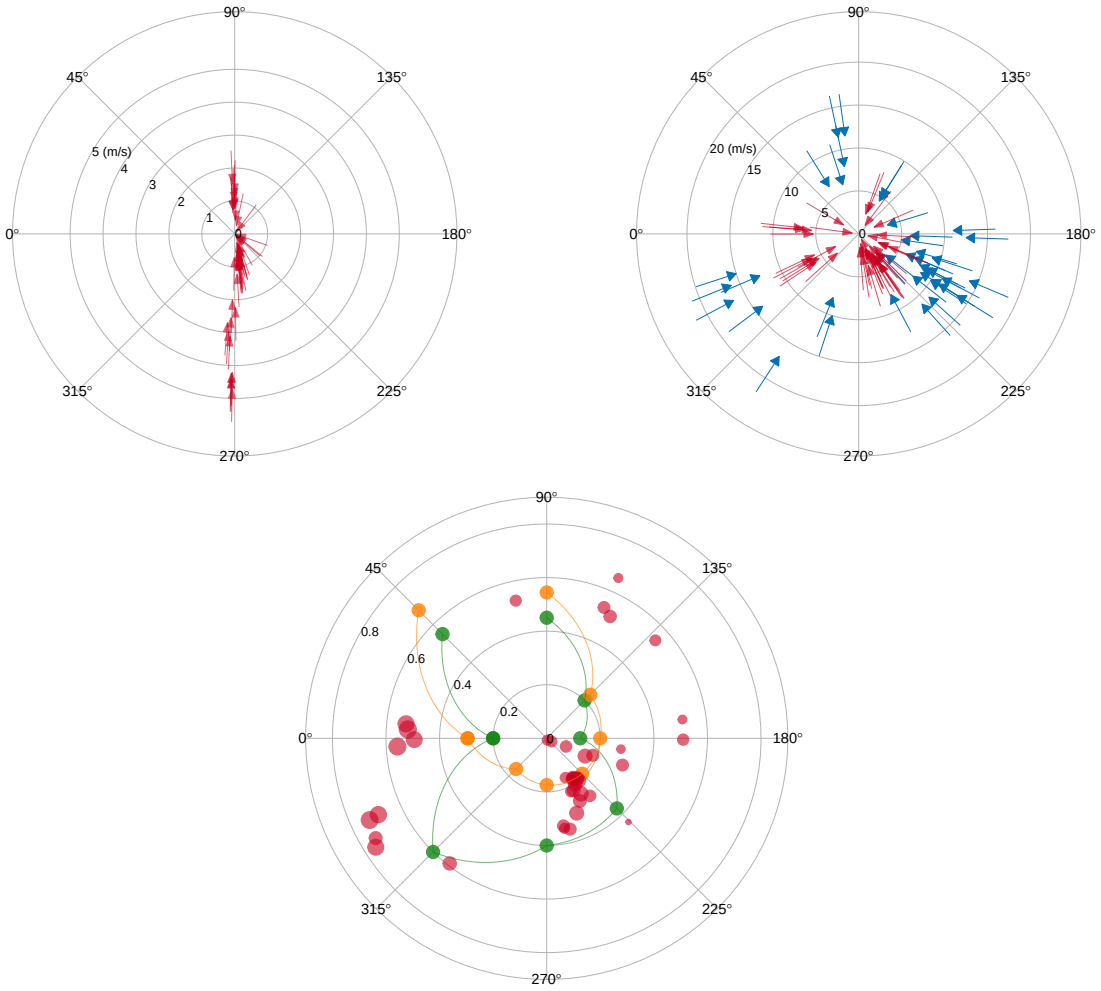

Figure 6: Wind data for individual tests. Top Left: Mean wind speed, $\bar{U}_l$ and incidence angle, θ_l, measured local to the opening taken as local conditions at the opening. Top Right: $\bar{U}_r$ and θ_r measured at 6.0 metres above roof level (shown in red) and data taken from the nearby met station, Cork Airport (shown in blue), for the same 44 test periods. Bottom: Ratio of U_l/U_r for each test according to θ_r, with size of point proportional to $\bar{U}_r$. Warren wind tunnel measurements shown in green, Adams equation for estimating U_l/U_r shown in orange.

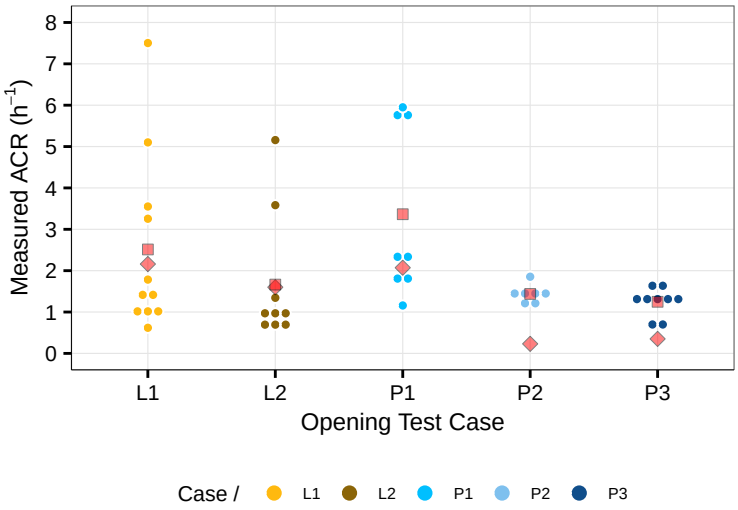

Figure 7: Measured mean ACR values presented using discrete categories according to opening type and case (see figure 2). Also shown is the sample mean (red square), standard deviation (red diamond).

- There is a much wider spread of values for the slot louvre cases with the plain opening cases displaying consistency about values between 0.035-0.04. These values are similar to those published by Warren for a turbulent flow field.

4.3 Characteristics of the wind at the opening

Chu et al (2011)recently demonstrated that the dimensionless exchange rate parameter can have different values depending on the wind incidence angle. This is due to differing air exchange mechanisms generated . How these different airflow exchanges interact with any buoyancy forces present depends to some extent on the magnitude of the buoyancy force which itself is influenced by the geometry of the opening. The spectral characteristic of the velocity, and by extension the airflow, in the opening can reflect whether or not the interaction is affected by a particular change in opening geometry and design. As windward and leeward conditions exhibit different local airflow exchange schemes, results from windward/leeward tests with similar boundary conditions for L1 & P1 were identified and compared, (Table 6), to investigate how the the slot louvre influences the local $U_l - \Delta T$ relationship. To identify these we used the local 1D turbulence intensity I_l, (Eq. (13)), mean local wind speed $\bar{U}_l$, mean wind incidence angle $\bar{\theta}_r$ and Archimedes number, $Ar^{0.5}$. Turbulence Intensity, I, is defined as the standard deviation of longitudinal wind speed, σ_U, normalised with the mean wind speed, $\bar{U}$.

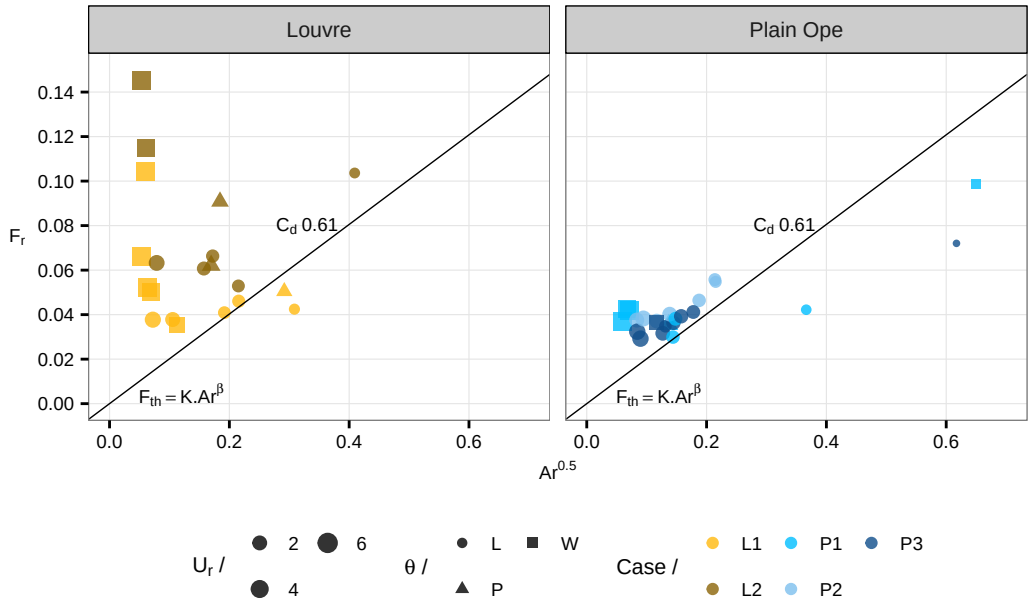

Figure 8: Reference dimensionless exchange rate parameter, F_r Vs adjusted Archimedes Number, $Ar^{0.5}$. Data categorised according to opening type and case (Figure 2)

Table 6: Test summary data for L1 & P1 tests with similar high and medium/low turbulence boundary conditions

Case	I_o	Test	A_o	$\bar{U}_l$	I_l	θ_r	$Ar^{0.5}$	$\bar{I}_o$	$\bar{U}_o$	ACR
$(-)$	$(-)$	$(-)$	(m^2)	(ms^{-1})	$(\%)$	(deg)	$(-)$	$(\%)$	(ms^{-1})	(h^{-1})
P1	High	10	0.228	2.62	49	**359**	0.067	7.7	0.42	5.7
L1	High	07	0.107	3.35	69	**4**	0.054	20.8	0.81	5.1
P1	Low	14	0.228	0.30	11	**188**	0.367	8.7	0.10	1.2
L1	Low	15	0.107	0.04	15	**213**	0.192	10.9	0.07	0.9

$$I = \frac{\sigma_U}{\bar{U}} \tag{13}$$

To characterise velocity in a turbulent flow field Taylor (1938) proposed spectral analysis as a technique for studying the distribution of energy at different eddy scales. The total energy distribution in the power spectrum scales as a function of the frequency power exponent. Kolmogorov proposed $\beta = -5/3$ in Eq. (14), for a theoretical isotropic turbulent fluid (1941).

$$S(\omega) \propto \omega^{-\beta} \tag{14}$$

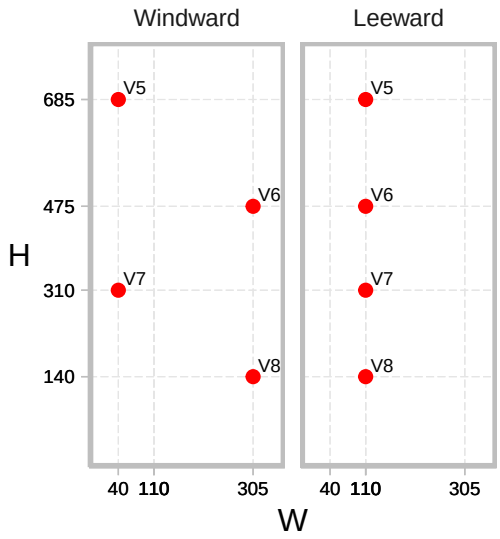

Figure 9: Opening elevations showing dimensions of anemometer locations during windward and leeward tests from Table 2. Note: the origin (0,0) represents the south corner of the opening when considered in plan, i.e. the bottom right in Figure 2

Explicit to building applications Maloniwski (1971) demonstrated that only an eddy with a scale smaller than the opening size can penetrate into the room. More recently, researchers have used power spectra to investigate whether the characterstics of the airflow as it undergoes some change owing to the surrounding environment is "mechanical" or "natural" showing this is a function of mean wind speed (Ouyang et al. 2006; Gao et al. 2015; Larsen and Heiselberg 2008). The discrete power spectrum, $S(\omega_j)$, can provide this information giving the energy distribution by decomposing the sampled time series wind data into various component frequencies. For non periodic processes the discrete fourier transform, $d(\omega_j)$, Eq. (15), is used to reconstruct an approximate representation of the continuous power spectrum from sampled measurement data with the power spectrum obtained from the squared magnitudes of the fourier coefficients, Eq. (16). Using velocity data at locations shown in Figure 9, The Cooley - Tukey Fast Fourier Transform (Cooley and Tukey 1965) was implemented to complete this transformation. Figure 10 shows log transformed power spectra for the boundary velocity and the opening locations for tests in Table 6 (different locations for windward and leeward were chosen in part due to the varying nature of air exchange at the opening).

$$d(\omega_j) = n^{-1/2} \sum_{t=1}^{n} x_t e^{-2\pi i \omega_j t}, \quad for \quad j = 0, 1, \cdots, n-1. \tag{15}$$

$$S(\omega_j) = \mid d(\omega_j) \mid^2 \tag{16}$$

For location V6 and V8 the plain opening displays similiar distributions of energy for both leeward and windward tests, both showing quite flat profiles, with the energy spread more evenly across all scales. No noticeable difference exists in the nature of the wind between all 4 locations in the opening. The steep distribution of energy at the higher frequencies in the boundary wind for both windward and leeward is redistributed to the lower frequencies as it passes through the opening. No energy above $1.0m^2s^{-1}$ was seen in the opening while the boundary wind contained values upwards of $50.0m^2s^{-1}$. For the slot louvre a different wind characteristic is clearly visible depending on $\bar{\theta}_r$ as well as measurement location. A steeper distribution is visible near the trailing edge of the opening where the turbulent jet is likely deflected inwards. At location V8 we see energy at scales comparable to those in the boundary wind spectrum though at lower frequencies. The windward and leeward tests have different spectrum for the slot louvre with a more natural characteristic for the windward test. Both P1 and L1 cases have similar power spectra for leeward conditions with a slight variation in the slope, β, of the distribution.

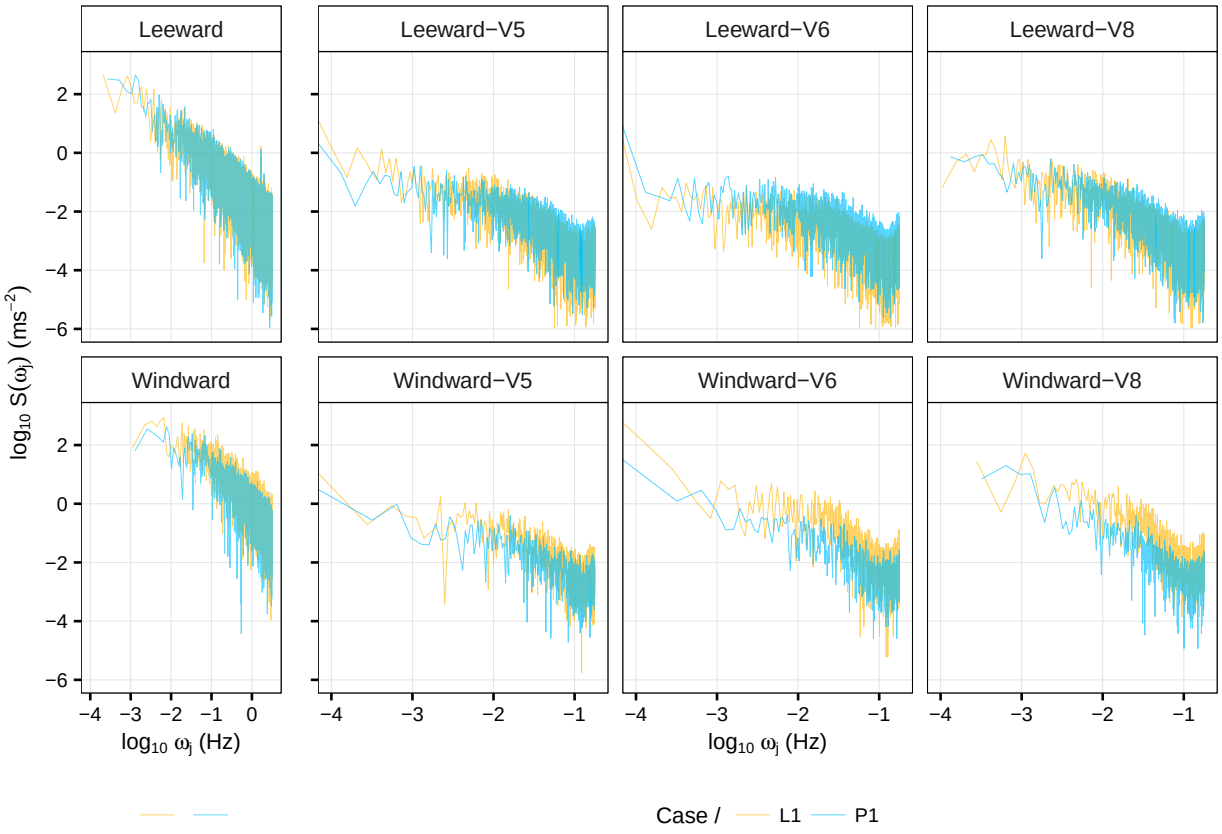

Figure 10: Power spectra for wind velocity measured at the opening for high turbulence (windward) and low turbulence (leeward) tests. Opening boundary spectra (U_l) shown to the left. Top: Comparison of spectra for leeward tests & cases L1 and P1. Bottom: Windward tests. Axes are log transformed.

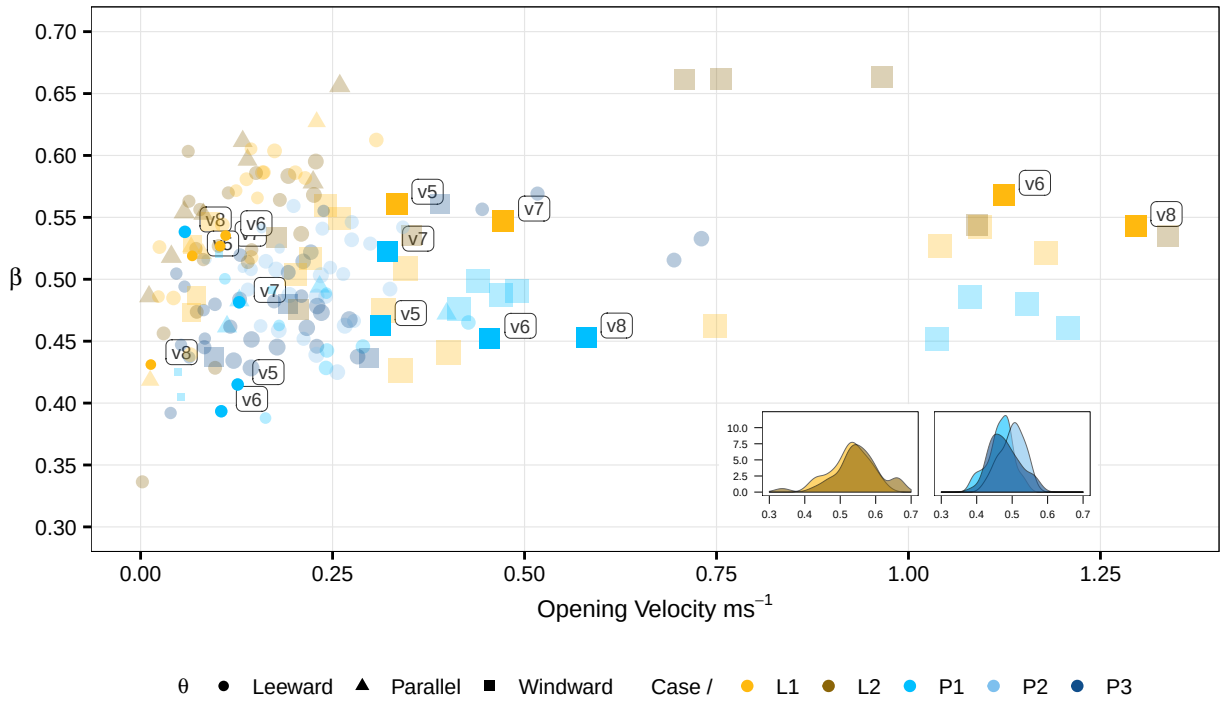

Figure 11: β for all velocity measuring positions within the opening according to mean test opening velocity categorised according to opening case tested. Size of each data point relative to mean boundary wind speed, U_l. Values used to calculate mean opennig conditions in Table 6 coloured darker. Kernel density estimates for each case also shown.

Figure 11 shows β values as a function of the local mean velocity in the opening, $\bar{U}_o$, at all 4 measuring locations during each test (176 values in total for 44 tests). β is calculated as the negative slope of the OLS model fit $lg(S(\omega_j)) = \beta \cdot lg(\omega_j)$ within the frequency range $0.01Hz < \omega_j < 1.0Hz$. The points representing the 4 positions in the 4 different tests in table 6 are specifically highlighted. The Louvre measurements show slightly higher values for both high turbulence tests (windward) and low turbulence tests (leeward) compared with the plain opening. In general a similar pattern exists between the two different opening types, L and P, although the plain opening shows slightly flatter distributions of energy across the various opening velocities, particularly for low velocity leeward tests. The mean β for L cases is 0.534 while for P cases it is 0.481. For windward tests only these values are 0.532 and 0.473 respectively. These results are lower than published by previous researchers. However, the narrow, deep nature of the opening may also contribute to this marked change in the opening wind characteristics. The slot louvre may attenuate these effects somewhat by deflecting the incoming air using its concave profile. While the nature of the wind seems relatively similar there is more energy in the slot louvre cases suggested by Figure 10. Kernel Density estimates are also shown in Figure 11 showing the different distributions of β depending on opening case.

4.4 Boundary conditions influential to ACR

The non-dimensional analysis suggests that there exists a value of F_r for the slot louvre different to that recommended by previous researchers (P. R. Warren and Parkins 1985; Adams et al. 2014; Chu, Chen, and Chen 2011). Some dependancy on temperature might also exist for leeward test conditions with the slot louvre, even for the low opening height (Figure 8). To investigate the most suitable candidate set of boundary parameters for predicting ventilation rates with the slot louvre system we employ a sensitivity analysis using multiple linear regression (MLR) with bi-directional stepwise selection. This was completed using an efficient branch and bound algorithm from the leaps package in R (Lumley 2009). As a measure of fit we use the adjusted R-squared value, $\hat{R}^2$, correcting for undesirable effects from increasing the number of variables in the MLR model. We used Eq. (17) as the basis for the model:

$$y = a + \sum_{i=0}^{n} b_i x_i + \epsilon, \quad for \quad i = 0, 1, \cdots, n-1. \tag{17}$$

For the predictor variables, x_i, We used the empirical parameters $U_l A_o$ & $U_r A_o$, the wind incidence angle $\bar{\theta}$ and the envelope temperature difference ΔT_{ie}. Table 7 summarises the results from the stepwise selection search process for the full slot louvre data set (all directions), Windward tests only and Leeward tests only. Only the best three candidate combinations for each variable are presented giving ten models in total for

each (some combinations are amongst the best three for more than one variable). For the all wind directions combined we obtain $\hat{R}^2 = 0.871$ for the combination $[U_l A_o, \theta_r]$ with a marginal reduction when $U_r A_o$ is added to the model. When we omit both θ and ΔT_{ie} we have $\hat{R}^2 = 0.829$ for $U_l A_o$ and $\hat{R}^2 = 0.836$ for $U_r A_o$ arguably an acceptable decrease for a simplified candidate set. The windward data set shows strong correlations with better predictive ability when using $U_r A_o$ compared with all wind diredctions. $U_l A_o$ combined with various parameters still gives the best prediction ability with $\hat{R}^2 = 0.914$ when θ and ΔT are included. The leeward study displays the strongest correlations in general with ΔT featuring in 5 of the models compared with the previous data sets and $U_r A_o$ giving the best predictions as opposed to $U_l A_o$ suggesting a more disturbed local velocity pattern when the wind is leeward. In terms of prediction ability, $U_l A_o$ and $U_r A_o$ have strong correlations even when considered in isolation from other parameters.

Table 7: Results from stepwise selection process for four boundary parameters U_l, U_r, θ and δT with three different sets of experimental test results, All wind directions, windward only & leeward only.

	All θ			**Windward θ**			**Leeward θ**	
No	**subset**	$\hat{R}^2$	**No**	**subset**	$\hat{R}^2$	**No**	**subset**	$\hat{R}^2$
A1	$U_l A_o, \theta$	0.871	W1	$U_l A_o, \theta, \Delta T$	0.914	L1	$U_r A_o, \Delta T$	0.969
A2	$U_l A_o, U_r A_o, \theta$	0.866	W2	$U_l A_o, U_r A_o, \theta, \Delta T$	0.909	L2	$U_r A_o, \theta, \Delta T$	0.967
A3	$U_l A_o, \theta, \Delta T$	0.866	W3	$U_l A_o, \theta$	0.856	L3	$U_r, \Delta T$	0.967
A4	$U_l A_o, U_r A_o, \theta, \Delta T$	0.864	W4	$U_r A_o, \theta, \Delta T$	0.850	L4	$U_l A_o, U_r A_o, \Delta T$	0.965
A5	$U_l A_o, U_r A_o$	0.857	W5	$U_r A_o$	0.841	L5	$U_r A_o, \theta$	0.965
A6	$U_l A_o, U_r A_o, \Delta T$	0.849	W6	$U_r A_o, \theta$	0.840	L6	$U_l A_o, U_r A_o, \theta, \Delta T$	0.963
A7	$U_l A_o, \Delta T$	0.839	W7	θ,	0.835	L7	$U_r A_o$	0.942
A8	$U_r A_o$	0.836	W8	$U_l A_o$	0.827	L8	$U_l A_o, U_r A_o$	0.939
A9	$U_l A_o$	0.829	W9	$U_l A_o, U_r A_o, \theta$	0.826	L9	θ	0.882
A10	θ	0.697	W10	$U_l A_o, U_r A_o$	0.812	L10	$U_l A_o$	0.725

4.5 Comparison with experimental data

Experimental results have shown that, with comparable overall facade opening dimensions dimensions, the slot louvre system performs comparably well to the plain opening. Existing single sided correlations have been developed from studies using either a plain opening or some form of conventional window geometry. To

investigate the suitability of these correlations a comparison of those in Table 5 with experimental data was completed, presented in Figure 12. Axes are log transformed to accommodate the wide range of predictions from various correlations and 25% error range is also shown. Table 8 presents correlation error metrics using root mean square error (rmse), mean absolute percentage error (mape) and the standard R^2 goodness of fit value (R-sq). The Caciolo correlation uses the simplified single coefficent of $F_r = 0.025$, from Warren (1985) for windward tests and their own correlation for leeward tests. The Warren correlation, based on $F_l = 0.1$ and includes the U_l/U_r ratio as a function of $\bar{\theta}$.

4.5.1 Plain Opening

For case P1 all correlations except Argiriou generally predicted low velocity, leeward tests within to within 25% error and provided predictions of high velocity windward tests for this case also within this range (These tests had $U_l > 4.3ms^{-1}$). All correlations underpredicted P2 tests even though the level of underprediction varaied. Argiriou had the lowest mape at 21% with Warren having an mape of 22% when considering all P cases combined.

4.5.2 Slot Louvre

All correlations underpredicted almost all the case L2 tests particularly for the high wind speed windward tests. In some cases these underpredictions were substantial. For the low wind speed case L1 tests (which were predominantly leeward), except for Caciolo, correlations either predicted close to 25% or overpredicted ACR. All correlations except Warren systemically underpredicted windward tests. Warren had the lowest mape at 36% when considering all L cases combined and appeared to predict the L1 pattern adequately.

In general most correlations predicted the correct pattern for the P cases and for the L cases had gave large underpredictions for nearly all measured ACR. Figure 8 suggests most tests for cases L1 & L2 are wind dominant with shear mixing the most likely mechansim driving flow attenuating pressure driven flow due to temperature differences at the opening. For Q Warren's correlation selects the maximum value, $Q = \max [Q_w, Q_{th}]$, and therefore may not always necessarily use a correlation based on the appropriate theory. A better but less direct approach might be to consider an upper limit Ar, F_r range, beyond which a buoyancy correlation is selected. The sensitivity study in section 4.4 demonstrates a strong correlation with wind speed for the slot louvre for windward conditions and also for leeward conditions.

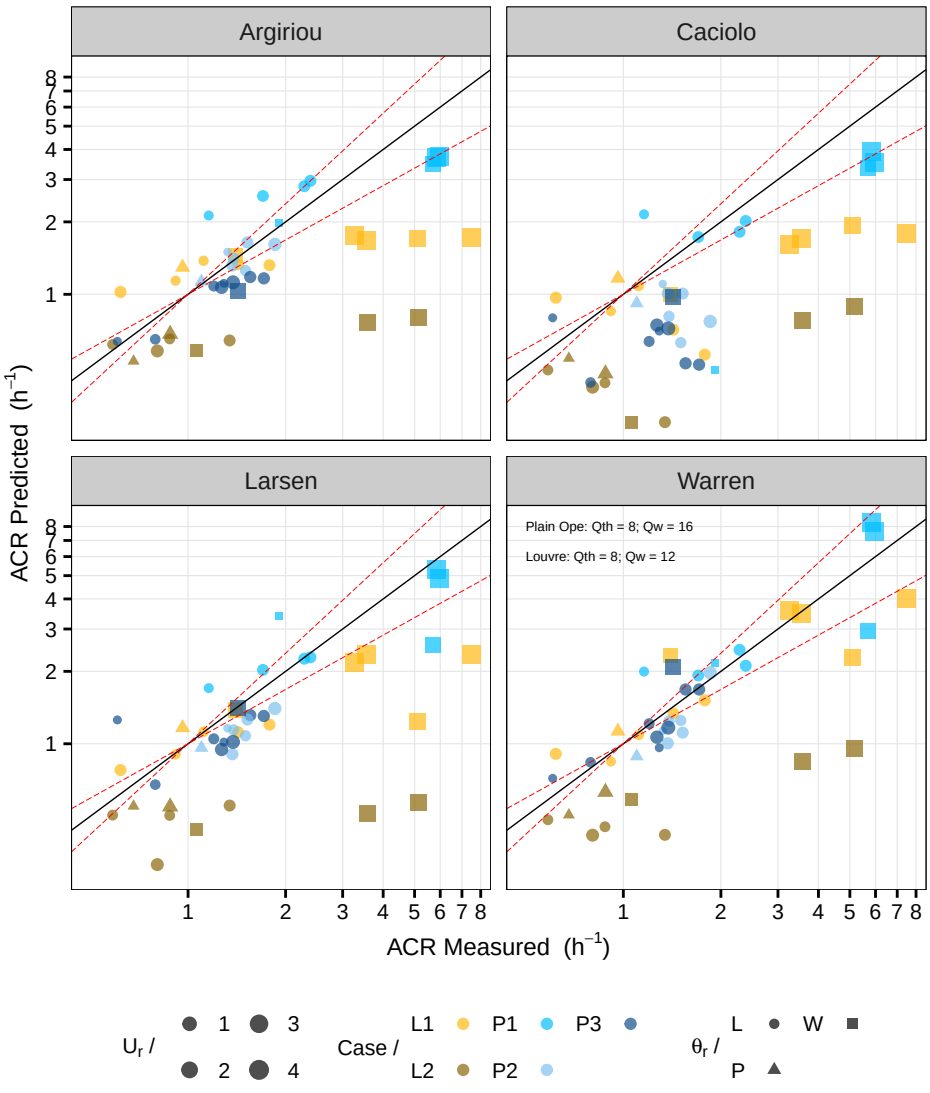

Figure 12: Comparison of existing correlations with measured ACR values for all tests. Axes are log transformed to accommodate large spread of predictions in some correlations. 25% error ranges shown as red dashed lines.

Table 8: Model metrics for existing correlations fit to measured ventilation rate data

Model	L rmse (ACR)	L mape (%)	L R-sq	P rmse (ACR)	P mape (%)	P R-sq
Warren	1.6	36	0.49	0.89	22	0.78
Argiriou	2	39	0.3	0.81	21	0.81
Larsen	1.9	39	0.33	0.86	28	0.7
Caciolo	2	48	0.51	1	43	0.81

5 Discussion

5.1 Sources of enhanced airflow exchanges

The slot louvre has comparable performance to a plain opening using the same overall facade opening dimensions and has substantially improved ACR performance for a comparable net free opening area. The existing models generally ACR within 25% error for plain openings. With such a narrow, deep opening (see dimensions in Figure 2) it is reasonable to suspect the existence of a strong jet deflection into the space with the resulting effects not accounted for. Hasama et al (2008) showed the depth of an opening is critical in determining the extent of the jet deflection and changes to the mixing layer characteristic in shear driven flow across an opening. Using a square opening of dimension D and an opening depth ratio $0.2D$ they show the existence of a large jet deflection (case-T). Taking $D \equiv l$ for the cases presented here we have a ratio of $0.44l$ which is substantially greater than their case T. This jet deflection may produce an aeration mechanism at the opening that wasn't predicted by existing correlations. Further, as most P2 and P3 tests were leeward where an additional 3 dimensional complicated flow that can develop, the models underpredicted these tests. However, In general the average prediction accuracy for the P cases is similar to that demonstrated in previous studies. The concave redirecting profile of the slot louvre suggests that the jet would be guided through an angle of approximately 90°as it enters the opening. This change in the entry angle of the jet could change the relationship between inflow and outflow as well as mixing in the shear layer. To confirm this further work investigating the spatial evolution of the jet across the slot louvre is needed. Further to this there has been some research investigating the impingement of a slot jet on a curved surface, often normal to the axis of curvature. For example it has been shown by Thomann (1968) that for flow over a concave surface centripetal forces can cause Taylor - Gortler vortices to develop and these can signficiantly increase the momentum and energy exchange near the wall. Gau (1991) also demonstrated the development of Taylor-Gortler when an air jet is flowing across a concave surface. Choi et al (2000) measured jet flow characteristics for impinging and wall jet for semi circular concave surfaces. When we consider the concave shape of the slot louvre and the

resulting guiding of the deflected jet this may promote a more efficient mixing with the aquisecent indoor air than with the plain opening. The investigation of these phenomena is required to further verify their existence as the source of more efficient airflow exchanges at the opening with the slot louvre.

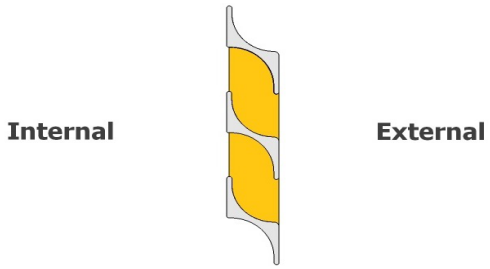

Figure 13: Section of slot louvre showing concave profile, with flow travelling normal to this profile when parallel along envelope. Airflow path shown coloured.

5.2 Dimensionless macroscopic ACR for slot louvres

For the opening height considered it has been shown that the slot louvre was wind dominant under all windward conditions and some leeward conditions. The results from the sensitivity study show that, with the same candidate set of boundary parameters, equally stong correlations exist for both windward and leeward tests depending on whether U_l or U_r was included with ΔT . When all tests are included, U_l, U_r & θ were shown to have the strongest correlation with ACR values with a marginal decrease when ΔT was included. When using U_l or U_r alone with A_o strong correlations were still present. Consequently, to predict macroscopic wind driven ACR through these types of openings, we suggest a simplified correlation similar to Warren. Table 9 presents values for the dimensionless parameter F_r. These were calculated using the regression variable b_i in equation 15 from section 4.4 above to estimate F_r values setting x equal to the empirical parameter $U_r A_o$. Values are included for the plain opening cases (P1, P2 & P3) for comparison purposes (and are themselves generally in line with the findings of Warren (1985) and recently discussed by Chu et al (2015)). From Table 9 and Figure 12 the lower limit value of 0.25 for the ratio U_l/U_r suggested by Warren may be too low for the louvre profile studied and appears highly dependant on the local surroundings.

Table 9: Values for F_r according to different wind directions, windward and leeward (Parallel U_r taken as leeward or windward depending on θ_r). No windward tests for P2 were recorded. Values based on combining all L cases and all P cases also shown. All values rounded to two significant digits.

Case	F_r **(Windward only)**	F_r **(Leeward only)**	F_r **(All Directions)**
L1	0.067	0.039	0.061
L2	0.131	0.063	0.107
P1	0.041	0.035	0.040
P2	-	0.041	-
P3	0.037	0.034	0.034
L1 & L2	0.073	0.043	0.067
P1, P2 & P3	0.040	0.036	0.039

Table 10: % change in F_r between different opening cases with comparable geometry characteristics. Wind direction used for each comparison based on available data from field study.

Cases	**Comparable Geometry**	**% change in** F_r	**Wind Direction**
L1 ~ P2	A_o, $(H_{o,L1} = H_{o,P2})$	-5%	Leeward
L1 ~ P3	A_o, $(W_{o,L1} = W_{o,P3})$	+79%	All
L1 ~ P1	H_o, W_o	+53%	All
L2 ~ P2	H_o, W_o	+54%	Leeward

In fact even setting this value to 0.35 for a turbulent flow field will still underpredict ACR. When using U_r directly to predict ventilation rates for the slot louvre an alternative F_r value should be further considered. Table 10 shows that for similar overall facade aperture dimensions a 53% efficiency improvement was observed and a higher F_r value, potentially dependant on wind direction should reflect this. When all L cases are combined a value of 0.067 for F_r is observed while a value of 0.039 for P cases is observed and close to that of 0.035.

6 Conclusion

It was found that little experimental field study data is currently reported in literature for architectural slot louvre ventilation components even though these are in wide use in passively ventilated buildings. A field study was completed that demonstrated improved dimensionless exchange rate performance for a concave profiled slot louvre when compared with a plain opening. There were larger increases in the value of F_r for windward incidence angles versus leeward. A value in the range 0.04 - 0.07 for F_r is suggested when modelling slot louvre systems having similar characteristics though this depends on the depth of opening

(as this likely plays a role in the performance of the louvre jet deflection action). There appears to be a clear enchancement taking place for windward tests with a modified velocity characteristic in the opening when using the slot louvre and the concave nature of the louvre profile is considered important in this regard. Existing correlations better predicted the plain opening P cases with mape values in the range 21% - 28% for 3 of the 4 correlations investigated. There were larger mape values for the slot louvre ACR, in the range 36% - 48%. The improved dimensionless exchange rate performance suggests there is an increased heat removal potential with these components that should be considered when considering various purpose provided opening types for a building operating with single sided ventilation. Further investigations are needed to isolate the exact phenomena contributing to the improved macroscopic ACR and F_r.

References

Adams, K., E. Arens, D. Banks, S. Brunswick, G. Carrilho da Graca, N. Daish, S. Dutton, et al. 2014. "Natural Ventilation For Energy Savings In California Commercial Buildings." California: University of California, UC San Diego.

Aflaki, A., N. Mahyuddin, and M. R. Baharum. 2016. "The Influence of Single-Sided Ventilation Towards the Indoor Thermal Performance of High-Rise Residential Building: A Field Study." *Energy and Buildings* 126: 146–58. http://dx.doi.org/10.1016/j.enbuild.2016.05.017.

Argiriou, A. A., C. A. Balaras, and S. P. Lykoudis. 2002. "Single-sided ventilation of buildings through shaded large openings." *Energy* 27 (2): 93–115. doi:10.1016/S0360-5442(01)00058-5.

Artmann, N., H. Manz, and P. Heiselberg. 2007. "Climatic potential for passive cooling of buildings by night-time ventilation in Europe." *Applied Energy* 84 (2): 187–201. doi:10.1016/j.apenergy.2006.05.004.

ASTM. 2011. "ASTM E741-11 Standard Test Method for Determining Air Change in a Single Zone by Means of a Tracer Gas Dilution." *ASTM International* 00 (2006): 1–18. doi:10.1520/E0741-11.Copyright.

Belleri, A., R. Lollini, and S. M. Dutton. 2014. "Natural ventilation design: An analysis of predicted and measured performance." *Building and Environment* 81 (November). Elsevier Ltd: 123–38. doi:10.1016/j.buildenv.2014.06.009.

Caciolo, M., S. Cui, P. Stabat, and D. Marchio. 2013. "Development of a new correlation for single-sided natural ventilation adapted to leeward conditions." *Energy & Buildings* 60. Elsevier B.V.: 372–82. doi:10.1016/j.enbuild.2013.01.024.

Caciolo, M., P. Stabat, and D. Marchio. 2011. "Full scale experimental study of single-sided ven-

tilation : Analysis of stack and wind effects." *Energy & Buildings* 43 (7). Elsevier B.V.: 1765–73. doi:10.1016/j.enbuild.2011.03.019.

Chen, Q. 2009. "Ventilation performance prediction for buildings: A method overview and recent applications." *Building and Environment* 44 (4). Elsevier Ltd: 848–58. doi:10.1016/j.buildenv.2008.05.025.

Chiesa, G., and M. Grosso. 2015. "Geo-climatic applicability of natural ventilative cooling in the Mediterranean area." *Energy and Buildings* 107. Elsevier B.V.: 376–91. doi:10.1016/j.enbuild.2015.08.043.

Choi, M., H. S. Yoo, G. Yang, J. S. Lee, and D. K. Sohn. 2000. "Measurements of impinging jet flow and heat transfer on a semi-circular concave surface." *International Journal of Heat and Mass Transfer* 43 (10): 1811–22. doi:10.1016/S0017-9310(99)00257-4.

Chu, C. R., R. H. Chen, and J. W. Chen. 2011. "A laboratory experiment of shear-induced natural ventilation." *Energy and Buildings* 43 (10). Elsevier B.V.: 2631–7. doi:10.1016/j.enbuild.2011.06.014.

Chu, C. R., Y. H. Chiu, Y. T. Tsai, and S. L. Wu. 2015. "Wind-driven natural ventilation for buildings with two openings on the same external wall." *Energy and Buildings* 108. Elsevier B.V.: 365–72. doi:10.1016/j.enbuild.2015.09.041.

Cockroft, J. P., and P. Robertson. 1976. "Ventilation of an enclosure through a single opening." *Building and Environment* 11 (1): 29–35. doi:10.1016/0360-1323(76)90016-0.

Cooley, J. W., and J. W. Tukey. 1965. "An Algorithm for the Machine Computation of the Complex Fourier Series." *Mathematics of Computation* 19: 297. doi:10.2307/2003354.

Cui, S., M. Cohen, P. Stabat, and D. Marchio. 2015. "CO2 tracer gas concentration decay method for measuring air change rate." *Building and Environment* 84 (January). Elsevier Ltd: 162–69. doi:10.1016/j.buildenv.2014.11.007.

Dascalaki, E., M. Santamouris, A. Argiriou, C. Helmis, D.N. Asimakopoulos, K. Papadopoulos, and A. Soilemes. 1996. "On the combination of air velocity and flow measurements in single sided natural ventilation configurations." *Energy and Buildings* 24 (2): 155–65. http://www.sciencedirect.com/science/article/pii/0378778896009735.

Dimotakis, P. E. 2005. "Turbulent Mixing." *Annual Review of Fluid Mechanics* 37 (1): 329–56. doi:10.1146/annurev.fluid.36.050802.122015.

Ekmekci, A., and D. Rockwell. 2003. "Self-sustained oscillations of shear flow past a slotted plate coupled with cavity resonance." *Journal of Fluids and Structures* 17 (8): 1237–45. doi:10.1016/S0889-9746(03)00073-2.

Florides, G.A, S.A Tassou, S.A Kalogirou, and L.C Wrobel. 2002. "Measures used to lower building

energy consumption and their cost effectiveness." *Applied Energy* 73 (3-4): 299–328. doi:10.1016/S0306-2619(02)00119-8.

Gao, R., W. Zhang, Y. Zhang, and A. Li. 2015. "Statistical Characteristics and Frequency Spectrum Analysis of Fan Induced Airflow Compared with Natural Winds." *International Journal of Ventilation* 14 (3): 273–88.

Gau, C., and C. M. Chung. 1991. "Surface Curvature Effect on Slot-Air-Jet Impingement Cooling Flow and Heat Transfer Process." *Journal of Heat Transfer* 113 (4): 858. doi:10.1115/1.2911214.

Gids, W. De., and H. Pfaff. 1982. "Ventilation rates and energy consumption due to open windows: A brief overview of research in the Netherlands." *Air Infiltration Review* 4 (1): 4–5.

Hasama, T., S. Kato, and R. Ooka. 2008. "Analysis of wind-induced inflow and outflow through a single opening using LES & DES." *Journal of Wind Engineering and Industrial Aerodynamics* 96: 1678–91. doi:10.1016/j.jweia.2008.02.005.

Hughes, Ben Richard, John Kaiser Calautit, and Saud Abdul Ghani. 2012. "The development of commercial wind towers for natural ventilation: A review." *Applied Energy* 92. Elsevier Ltd: 606–27. doi:10.1016/j.apenergy.2011.11.066.

Koffi, J., M. El Mankibi, E. Gourdon, and R. Issoglio. 2015. "Assessment of single-sided ventilation with acoustic shutters on windows." *Building Simulation* 8 (6): 689–700. doi:10.1007/s12273-015-0246-3.

Kolmogorov, A. 1941. "The Local Structure of Turbulence in Incompressible Viscous Fluid for Very Large Reynolds' Numbers." *Akademiia Nauk SSSR Doklady* 30: 301–5.

Kolokotroni, M, and a Aronis. 1999. "Cooling-energy reduction in air-conditioned offices by using night ventilation." *Applied Energy* 63 (4): 241–53. doi:10.1016/S0306-2619(99)00031-8.

Kolokotroni, Maria, and Peter Warren. 2008. "Building Advent: Building Advanced Ventilation technological examples to demonstrate materialised energy savings for indoor air quality and thermal comfort." In *Proceedings Indoor Air*. Copenhagen, Denmark.

Kolokotroni, Maria, V Kukaida, and E Perera. 1996. "NATVENT - European project on overcoming technical barriers to low-energy natural ventilation." In *Proceedings CIBSE/ASHRAE Joint National Conference*, 36–41. Sept. Harrogate, UK.

Larsen, T. S., and P. Heiselberg. 2008. "Single-sided natural ventilation driven by wind pressure and temperature difference." *Energy and Buildings* 40 (6): 1031–40. doi:10.1016/j.enbuild.2006.07.012.

Lee, D. S., S. J. Kim, Y. H. Cho, and J. H. Jo. 2015. "Experimental study for wind pressure loss rate

through exterior venetian blind in cross ventilation." *Energy and Buildings* 107. Elsevier B.V.: 123–30. doi:10.1016/j.enbuild.2015.08.018.

Lumley, T. 2009. *Leaps: Regression Subset Selection*. https://CRAN.R-project.org/package=leaps.

Ma, Z., P. Cooper, D. Daly, and L. Ledo. 2012. "Existing building retrofits: Methodology and state-of-the-art." *Energy and Buildings* 55 (August). Elsevier B.V.: 889–902. doi:10.1016/j.enbuild.2012.08.018.

Malinowski, H. 1971. "Wind Effect on the air movement inside buildings." In *Third International Conference on Wind on Buildings and Structures*, 125–34. Tokyo.

Mara, T. G. 2014. "Influence of Solid Area Distribution on the Drag of a Two-Dimensional Lattice Frame." *Journal of Engineering Mechanics* 140 (3): 644–49. doi:10.1061/(ASCE)EM.1943-7889.0000681.

Moosavi, L., N. Mahyuddin, N. Ab Ghafar, and M. Azzam Ismail. 2014. "Thermal performance of atria: An overview of natural ventilation effective designs." *Renewable and Sustainable Energy Reviews* 34: 654–70. doi:10.1016/j.rser.2014.02.035.

Okuyama, H., and Y. Onishi. 2012. "Uncertainty analysis and optimum concentration decay term for air exchange rate measurements: Estimation methods for effective volume and infiltration rate." *Building and Environment* 49 (1). Elsevier Ltd: 182–92. doi:10.1016/j.buildenv.2011.09.018.

Ouyang, Q., W. Dai, H. Li, and Y. Zhu. 2006. "Study on dynamic characteristics of natural and mechanical wind in built environment using spectral analysis." *Building and Environment* 41: 418–26. doi:10.1016/j.buildenv.2005.02.008.

O'Sullivan, P. D., and M. Kolokotroni. 2014. "Time-averaged Single Sided Ventilation Rates and Thermal Environment in Cooling Mode for a Low Energy Retrofit Envelope." *International Journal of Ventilation* 13 (2): 153–68. doi:10.5555/2044-4044-13.2.153.

O'Sullivan, Paul D, and Maria Kolokotroni. 2016. "Non dimensional analysis and characterisation of driving forces for a single sided slot louver ventilation system." *International Journal of Ventilation* 14 (4): 335–48. doi:10.1080/14733315.2016.11684091.

Psomas, T., P. Heiselberg, K. Duer, and E. Bjørn. 2016. "Overheating risk barriers to energy renovations of single family houses: Multicriteria analysis and assessment." *Energy and Buildings* 117. Elsevier B.V.: 138–48. doi:10.1016/j.enbuild.2016.02.031.

Ramponi, Rubina, Adriana Angelotti, and Bert Blocken. 2014. "Energy saving potential of night ventilation: Sensitivity to pressure coefficients for different European climates." *Applied Energy* 123. Elsevier Ltd: 185–95.

578 doi:10.1016/j.apenergy.2014.02.041.

579 Roulet, C. A. 2007. *Ventilation and Airflow in Buildings: Methods for Diagnosis and Evalua-*
580 *tion (BEST (Buildings, Energy and Solar Technology))*. Routledge. http://www.amazon.co.uk/
581 Ventilation-Airflow-Buildings-Evaluation-Technology/dp/184407451X.

582 Sever, A. C., and D. Rockwell. 2005. "Oscillations of shear flow along a slotted plate: small- and large-scale
583 structures." *Journal of Fluid Mechanics* 530: 213–22. doi:10.1017/S0022112005003721.

584 Sherman, M. 1990. "Tracer Gas Techniques for Measuring Ventilation in a Single Zone." *Building and*
585 *Environment* 25 (4): 365–74.

586 Tang, Y., X. Li, W. Zhu, and P. Lun Cheng. 2016. "Predicting Single-sided Airflow Rates Based
587 on Primary School Experimental Study." *Building and Environment* 98. Elsevier Ltd: 71–79.
588 doi:10.1016/j.buildenv.2015.12.021.

589 Taylor, G. I. 1938. "The Spectrum of Turbulence." In *Proceedings of the Royal Society of London Series a,*
590 *Mathematical and Physical Sciences*, 476–90. The Royal Society.

591 Thomann, H. 1968. "Effect of Streamwise Wall Curvature on Heat Transfer in a Turbulent Boundary Layer."
592 *Journal of Fluid Mechanics* 33 (02): 283–92. doi:10.1017/S0022112068001308.

593 Van der Mass, J. 1992. "Airflow through large openings in buildings (subtask 2): IEA Annex 20 : Air Flow
594 Patterns within Buildings:"

595 Wang, H., and Q. Chen. 2012. "A new empirical model for predicting single-sided , wind-driven natural
596 ventilation in buildings." *Energy & Buildings* 54. Elsevier B.V.: 386–94. doi:10.1016/j.enbuild.2012.07.028.

597 Warren, P. R., and L. M. Parkins. 1985. "Single-sided ventilation through open windows." *ASHRAE SP49*,
598 no. 1. http://www.ornl.gov/sci/buildings/2012/1985 B3 papers/015.pdf.

599 Yamanaka, T., H. Kotani, K. Iwamoto, and M. Kato. 2006. "Natural, wind-forced ventilation caused by
600 turbulence in a room with a single opening." *International Journal of Ventilation* 5 (1): 179–87.